

Acquiring Human-Like Mechanics Intuition from Scarce Observations via Deep Reinforcement Learning

Jingruo Peng¹, Shuze Zhu^{*1}

¹Center for X-Mechanics, Institute of Applied Mechanics, Zhejiang University, Hangzhou 310000, China

*To whom correspondence should be addressed. E-mail: shuzezhu@zju.edu.cn

Abstract

Humans can infer accurate mechanical outcomes from only a few observations—a capability known as mechanics intuition. The mechanisms behind such data-efficient learning remain unclear. Here, we propose a reinforcement learning framework in which an agent encodes continuous physical observation parameters into its state and is trained via episodic switching across closely related observations. With merely two or three observations, the agent acquires robust mechanics intuition that generalizes accurately over wide parameter ranges, substantially beyond the training data—as demonstrated on the brachistochrone and a large-deformation elastic plate. We explain this generalization through a unified theoretical view: it emerges when the learned value function enforces Bellman consistency across neighboring task parameters, rendering the Bellman residual stationary with respect to physical variations. This induces a smooth policy that captures a low-dimensional solution manifold underlying the continuum of tasks. Our work establishes episodic switching as a principled route to artificial mechanics intuition and offers a theoretical link to similar generalization abilities in biological learners.

Keywords: reinforcement learning, mechanics, Bellman optimality, generalization, intuition learning

1. Introduction

Biological organisms acquire intelligent behavior through continual interaction with their environment. Reinforcement learning (RL) algorithms emulate such biological learning by optimizing actions through environmental interaction [1–3]. In humans, this ability to project the consequences of actions without direct trial-and-error is often described as “intuitive reasoning” [4], which in mechanical contexts we refer to as mechanical reasoning or mechanics intuition. Notably, humans can form robust mechanical intuitions from minimal exposure [5–9]. For example, a mason estimates beam deflection by inspection, and a carpenter judges a wooden beam’s load-bearing capacity from its grain and geometry. Cultivating such human-like, data-efficient mechanical insight is a pivotal challenge on the path toward artificial general intelligence [9–11].

Currently, the question of whether reinforcement learning is the right approach to artificial intelligence is debated. Critics point to limitations of current RL methods, arguing that richer priors, embodiment, or hybrid architectures are needed for general intelligence [12–17]. Yet, RL has also shown remarkable data-efficiency in domains like language modeling, where human feedback enables small models to outperform much larger ones [18–22]. Motivated by these potentials [23], we ask: can an RL agent develop human-like mechanics intuition from extremely limited observations?

To address this, we propose a simple yet effective RL framework centered on two core designs: (1) explicit encoding of continuous physical observation parameters (e.g., geometry, load) into the agent’s state representation, structuring the input to reflect the underlying parameter manifold; and (2) episodic observation-switching, a training protocol that repeatedly alternates the agent between tasks with neighboring parameters, encouraging a single strategy that generalize across local regions of this manifold. We adopt a train–freeze–execute scheme to rigorously evaluate generalization beyond the few observed task instances.

Our experiments on the brachistochrone and a large-deformation elastic plate show that switching across merely two or three similar observations yields a disproportionate expansion of the high-accuracy region compared to single-task training. Theoretically, we explain this gain through Bellman consistency: episodic switching enforces smoothness of the Bellman residual across parameters, which acts as an implicit regularizer, coupling policies and enabling robust

extrapolation.

This study demonstrates that RL, when suitably structured, can acquire a form of intuitive mechanical reasoning from scarce data. By encoding parameters and switching between related tasks, our method exploits inter-task similarity to induce human-like generalization. Practically, it offers a pathway to reduce data needs in physics-based RL; conceptually, it bridges data-efficient biological learning with algorithmic designs, showing how architectural and curricular choices can induce useful inductive biases.

2. Formulating Mechanics Problems as Reinforcement Learning Tasks

This method provides a complete, self-contained pipeline for converting mechanics problems into RL tasks and obtaining generalizable solutions through structured representation and episodic switching. The final solution is produced in a single forward pass of the learned policy, without iterative solver calls at test time, offering a computationally efficient route to data-driven physical intuition.

2.1 Problem Formulation as a Markov Decision Process

We formulate mechanics optimization problems—such as finding the brachistochrone curve or the equilibrium displacement field of an elastic plate—as fully observable, deterministic Markov Decision Processes (MDPs). The agent interacts with a physics simulator that embodies the governing mechanics functionals. The objective is to minimize a scalar physical quantity J (e.g., total travel time T or total potential energy E) through a sequence of actions that incrementally modify the candidate solution.

2.2. State Representation: Encoding Physical Observation Parameters

To condition the agent on the specific problem instance, we design a structured state representation that explicitly encodes continuous physical observation parameters ζ . At each collocation point i , the state vector is:

$$s_i = [x_i, y_i, \dots, \zeta_1, \zeta_2, \dots]^\top$$

where (x_i, y_i) are spatial coordinates, and the parameters ζ (e.g., endpoint coordinates \tilde{X} , \tilde{H} , load magnitude \tilde{P} , plate size \tilde{B} , orientation $\tilde{\theta}$) are repeated across all spatial locations as separate channels (Figure 1(a)). This structure allows convolutional layers to learn parameter-conditioned spatial operators while preserving translational equivariance.

The set of all ζ defines a smooth parameter manifold \mathcal{M} , where each point corresponds to a task instance. We denote ζ as the physical observation parameter and $s(\zeta)$ as the agent's state under observation ζ .

2.3. Action Space: Incremental Solution Updates

The action a_t at step t represents a local adjustment to the current solution field. For the brachistochrone, the action modifies the height $y(x)$ at a set of collocation points; for the elastic plate, it updates the displacement components (U, V, W) at each node. Actions are bounded to ensure physical plausibility and numerical stability. The state transition is deterministic: applying a_t updates the solution field accordingly, and the physics simulator re-evaluates the objective J .

2.4. Reward Function: Embedding the Physical Objective

The reward directly encodes the physical optimality criterion. For the brachistochrone, the reward encourages reduction of travel time $r_t = \text{sign}(T_{t-1} - T_t)$. For the elastic plate, the reward promotes decrease in total potential energy. $r_t = \text{sign}(E_{t-1} - E_t)$. Thus, each improvement in the physical objective yields a positive reward, aligning the RL agent's goal with the principle of least time or minimum potential energy.

2.5. Episodic Observation-Switching Protocol

To encourage generalization across nearby tasks, we employ an episodic observation-switching scheme (Figure 1(b)). Each training episode is associated with one fixed parameter value ζ_i . Upon episode termination, the environment switches to a different parameter ζ_j from the same local cluster (with $|\zeta_i - \zeta_j|$ small). The reward function uses the active ζ of the current episode. This forces the agent to learn policies that are effective across a neighborhood of parameters rather than overfitting to a single instance.

2.6. Network Architecture and Training

We use a dueling Deep Q-Network (DQN) with a convolutional backbone. The network takes the multi-channel state s and outputs the action-value function $Q_\theta(s, a)$. For the same task, all models share the same architecture and hyperparameters. Training is performed on a small, fixed set of parameter values $\zeta_1, \zeta_2, \zeta_3$ using experience replay and the switching protocol described above. Particularly, we operate on six training sets: three single-observation models

(each trained on one observation ζ_i , labeled as Single ζ_i), two double-observation models (each trained on a pair ζ_i, ζ_j via the switching protocol, labeled as Double ζ_i, ζ_j), and one triple-observation model (trained on all three observations, labeled Triple $\zeta_1, \zeta_2, \zeta_3$). The proximity (i.e., small $|\zeta_i - \zeta_j|$) of these selected parameters within the local cluster is fundamental. It embodies our core assumption: within a sufficiently small neighborhood of the parameter manifold, the optimal value function $Q^*(s, \zeta, a)$ and the corresponding policy vary smoothly. Our episodic switching protocol is explicitly designed to exploit and enforce this local smoothness prior, transforming it from an abstract assumption into a concrete training constraint.

2.7. Obtaining the Final Solution: Direct Execution of the Learned Policy

After training, the network parameters θ are frozen. The solution to a new problem instance with parameter ζ_{test} is obtained by directly executing the learned policy. Starting from an initial solution guess (e.g., a straight line or a flat plate), the agent follows the greedy policy derived from Q_θ : $a_t = \text{argmax}_a Q_\theta(s_t(\zeta_{test}), a)$ and interacts with the simulator for a fixed number of steps or until convergence. The final state reached after this rollout—i.e., the resulting curve $y(x)$ or displacement field (U, V, W) —is taken as the predicted solution to the physical problem. No further optimization, fine-tuning, or post-processing is applied. This “train–freeze–execute” pipeline ensures that generalization is evaluated purely on the basis of the learned policy, mimicking how a human expert would intuitively infer a solution across a broad range of previously unseen conditions from prior analogous experience (Figure 1(c)).

2.8. Evaluation of Generalization

Generalization is quantified by applying the frozen policy to a dense grid of unseen parameters ζ_{test} spanning a wide range. For each test case, the predicted solution is compared with a high-fidelity reference (analytic cycloid or Abaqus finite-element solution) using the coefficient of determination R^2 . A test point is considered successfully generalized if $R^2 \geq 0.90$. The union of all such points defines the generalized region in parameter space, whose size relative to the training set measures the method’s data efficiency and extrapolation capacity.

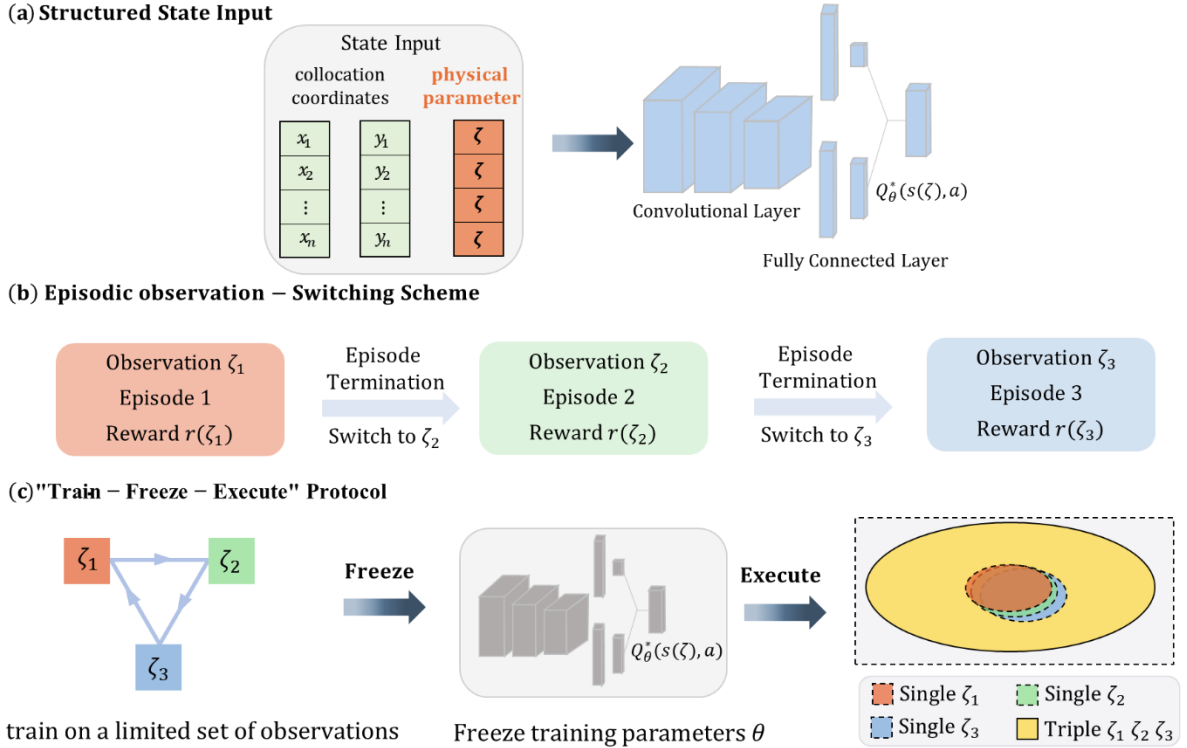


Figure 1. Schematic of episodic observation-switching training with structured state inputs. (a) Structured state input for continuous-field problems. The collocation coordinates (x_i, y_i) and physical observation parameters ζ are encoded into dedicated numerical channels and fed into a dueling Q-network to output the optimal action–value function $Q_\theta^*(s(\zeta), a)$. (b) Episodic observation-switching training scheme. Each episode is associated with a fixed observation ζ_i , and the observation is switched to ζ_j upon episode termination; the reward at each episode is defined as a function of the physical observation parameter associated with the active observation. (c) Train–freeze–execute protocol: the network is trained on a set of observations (e.g., $\zeta_1, \zeta_2, \zeta_3$), after which the learned parameters θ are frozen and the generalization interval is evaluated over an extended parameter range, revealing a disproportionate enlargement of high-accuracy region compared to single-observation training.

3. Computational Results

3.1 Brachistochrone

We validate our "train–freeze–execute" protocol on a canonical mechanics benchmark: the brachistochrone problem. In this task the agent predicts the time-optimal descent curve for a point particle subject to gravity that travels from the fixed start $(0,0)$ to a parametrized end point (\tilde{X}, \tilde{H}) and the analytic time-optimal solution is the cycloid and serves as our reference (Figure 2(a)). At each training iteration we compute the total traversal time T for the current candidate curve by numerical quadrature so that $T = \int_{x_0}^{x_1} \sqrt{\frac{1+(y')^2}{2gy(x)}} dx$ (with $y(x)$ measured as vertical drop). In our RL framework the physical law is directly embedded in the reward. At each step the agent proposes an incremental modification of the path and the total travel time T_t is recalculated. The reward is defined as $r_t = \text{sign}(T_{t-1} - T_t)$,

ensuring that updates that reduce time are positively reinforced. To allow the network to condition on the endpoint geometry, we encode the target endpoint coordinates (\tilde{X}, \tilde{H}) as two separate state channels. Each collocation point is therefore represented by a 4-channel state vector: $s = (x, y, \tilde{X}, \tilde{H})$, where (x, y) are the local spatial coordinates of the collocation points and (\tilde{X}, \tilde{H}) are constant across the nodes but presented as explicit input channels so the agent can learn endpoint-conditioned policies (Figure 2(b)).

We form local clusters of three neighboring observations corresponding to the physical observation parameter triplet $\zeta_1, \zeta_2, \zeta_3$. We compare six variants that share the same DQN backbone and hyperparameter set. After training, we freeze the network parameters and evaluate performance over a dense grid of unseen terminal points (\tilde{X}, \tilde{H}) spanning the two-dimensional parameter space. For every test endpoint we compute the network's predicted minimum-time trajectory y_{pred} and compare it to the cycloid y_{ref} . A test point is declared "generalized" when the coefficient of determination satisfies $R^2(y_{pred}, y_{ref}) \geq 0.90$. The generalized test points are aggregated to form a generalized region in the (\tilde{X}, \tilde{H}) parameter space. Figures 2(c – e) summarizes the generalized regions obtained for all models. The results show that the generalized region of the single-observation models is tightly concentrated and decays rapidly with increasing distance from the training observations, while the models trained on two neighboring observations yield an expansion of high-accuracy coverage relative to the single-observation unions. Incorporating a third neighboring observation further enlarges the generalized interval. Qualitatively, with more observations, the agent yields robust mechanics intuition over a substantially enlarged parameter domain, indicating a nonlinear amplification of generalization capability across the parameter manifold.

The brachistochrone experiments validate our central claim: from only a few highly similar observations, an RL agent can acquire a robust, endpoint-conditioned predictive policy that generalizes over a considerable portion of the continuous parameter space.

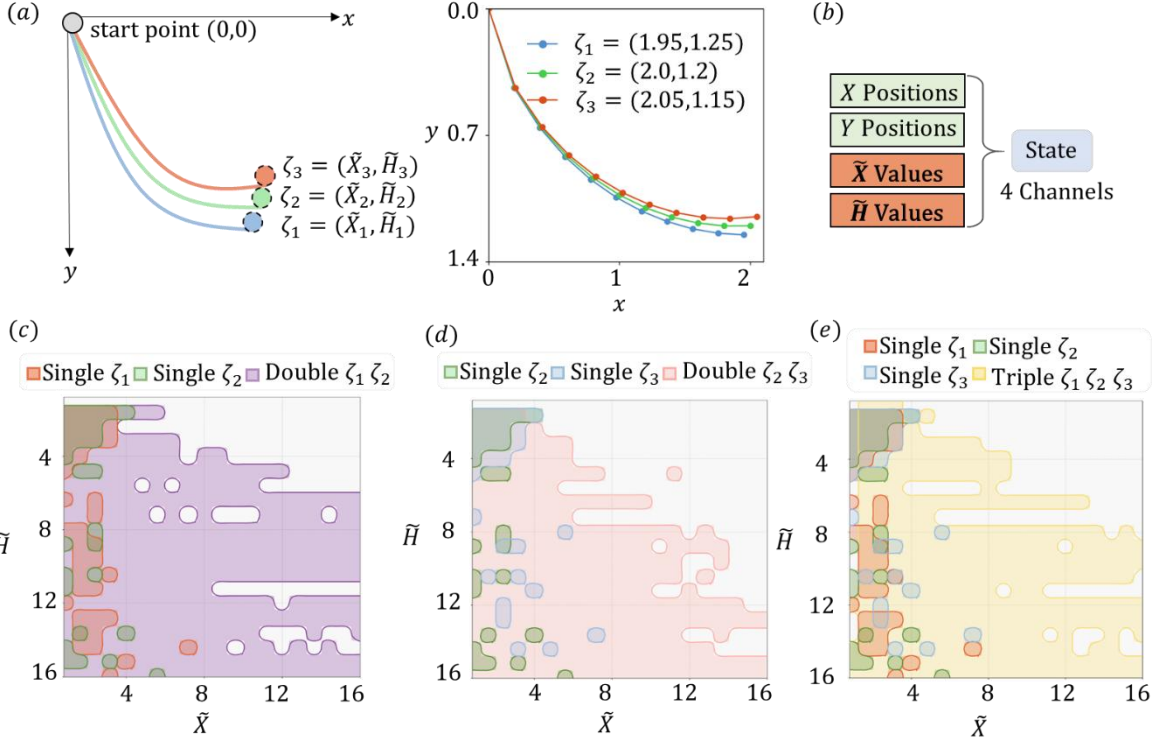


Figure 2. Generalization performance of episodic observation-switching training in the brachistochrone problem. (a) Brachistochrone problem with three closely spaced terminal points. The left panel illustrates the schematic setup with a common starting point $(0,0)$, while the right panel shows the corresponding exact brachistochrone trajectories associated with terminal coordinates (\tilde{X}, \tilde{H}) , which serve as training observations (gravity acts downward). (b) State representation for the brachistochrone problem, consisting of four channels: collocation coordinates along the x - and y -directions (X, Y), and the terminal point coordinates (\tilde{X}, \tilde{H}) . (c–e) Generalization performance comparison between single-observation training and episodic observation-switching training. (c) Generalization from individual observations ζ_1 and ζ_2 versus switching training on ζ_1, ζ_2 . (d) Analogous comparison for observations ζ_2 and ζ_3 . (e) Switching training on three observations $\zeta_1, \zeta_2, \zeta_3$ yields robust intuition over a substantially enlarged parameter domain, indicating a generalization gain beyond that achievable by individual observations.

3.2 Large-Deformation Elastic Plate

We next validate the proposed "train–freeze–execute" protocol on a large-deformation square plate problem to test the method's applicability to realistic continuum mechanics tasks. The physical setup is illustrated in Figure 3(a): a square plate of side length \tilde{B} and principal orientation $\tilde{\Theta}$ is clamped along its boundary and subject to a uniform transverse load \tilde{P} perpendicular to the plate surface. The agent's objective is to predict the full displacement field of the plate — both in-plane components along the x -axis $U(x, y)$ and along the y -axis $V(x, y)$, as well as the out-of-plane component $W(x, y)$ under the imposed boundary condition while accounting for geometric nonlinearity. In our implementation the constitutive response is linear elastic (constant Young's modulus and Poisson's ratio), consistent with the Abaqus reference solutions used for high-fidelity comparison. Accordingly, the system's total potential energy

E , comprising the internal strain energy and the external work of the applied load, is evaluated at each step by integrating the strain energy density over the plate domain together with the load contribution. This physical principle is embedded directly in the RL reward: at each training step, the total potential energy E_t of the current displacement field is computed, and a signed improvement reward is assigned as $r_t = \text{sign}(E_{t-1} - E_t)$, such that actions reducing the total potential energy are positively reinforced. This energy-based reward gives the agent a physically consistent objective that aligns with the principle of minimum potential energy for stable equilibria.

To condition the network on task parameters, \tilde{P} , \tilde{B} and $\tilde{\theta}$ are placed in dedicated state channels (Figure 3(b)) so that the per-collocation-point state vector contains six channels $s = (W, U, V, \tilde{P}, \tilde{B}, \tilde{\theta})$. Using this parameterized state representation, three distinct tasks are designed to probe the method's ability to exploit inter-task similarity. Task I (Varying Load Magnitude) concerns learning displacement fields under varying load \tilde{P} with fixed plate size $\tilde{B} = 100$ mm and orientation $\tilde{\theta} = 0^\circ$, while Task II (Varying Plate Size) involves learning size-dependent responses under varying \tilde{B} with fixed load $\tilde{P} = 1 \times 10^{-5}$ MPa and orientation $\tilde{\theta} = 0^\circ$, and Task III (Varying Orientation) focuses on learning orientation-dependent displacement patterns under varying $\tilde{\theta}$ with fixed load $\tilde{P} = 1 \times 10^{-5}$ MPa and plate size $\tilde{B} = 100$ mm. For each task, we construct a local cluster comprising three neighboring observations, denoted as $\zeta_1, \zeta_2, \zeta_3$ respectively. Figure 3(a) illustrates the degree of similarity among the three neighboring observations used in each task. Using the identical DQN backbone and hyperparameter set across variants, we train six model variants per task following the protocol described previously. Frozen models are then evaluated on dense test grids spanning large, previously unseen ranges of \tilde{P} , \tilde{B} and $\tilde{\theta}$ and accuracy is measured by the mean coefficient of determination $\bar{R}^2 = \frac{R_W^2 + R_U^2 + R_V^2}{3}$ against high-fidelity Abaqus references, with $\bar{R}^2 > 0.90$ denoting "generalized".

The experimental results demonstrate that the episodic switching training produces robust, observation-efficient mechanics intuition across all tasks. Across all three tasks, the agent trained with triple-observation switching accurately reproduces the reference finite-element solutions at the training configurations and, crucially, maintains high predictive fidelity when extrapolated far beyond the observed parameter range, as illustrated by the representative results in Figures 3(c – k). Despite substantial variations in load magnitude, plate size, or orientation, the learned displacement fields

remain in close agreement with the Abaqus solutions, demonstrating consistently strong generalization across distinct physical regimes. Figure 3(*l*) quantifies the more-than-additive expansion of generalization: single-observation training produces narrowly localized generalized regions near training points while double-observation training expands the generalized regions substantially, and triple-observation training yields near-global coverage across the sampled parameter axis in all tasks.

The elastic-plate experiments corroborate the brachistochrone findings: episodic switching training enables an RL agent to extract and exploit inter-task similarity in physics-governed problems, learning a smooth policy on the underlying parameter manifold, producing wide-ranging, human-like mechanics intuition from only a few neighboring observations. Having established the empirical effectiveness of our episodic observation-switching method across two distinct continuum mechanics problems, we now delve into the underlying mechanisms that enable such data-efficient generalization. The following sections provide a theoretical explanation from the perspectives of Bellman optimality, geometric learning, and algorithmic implementation.

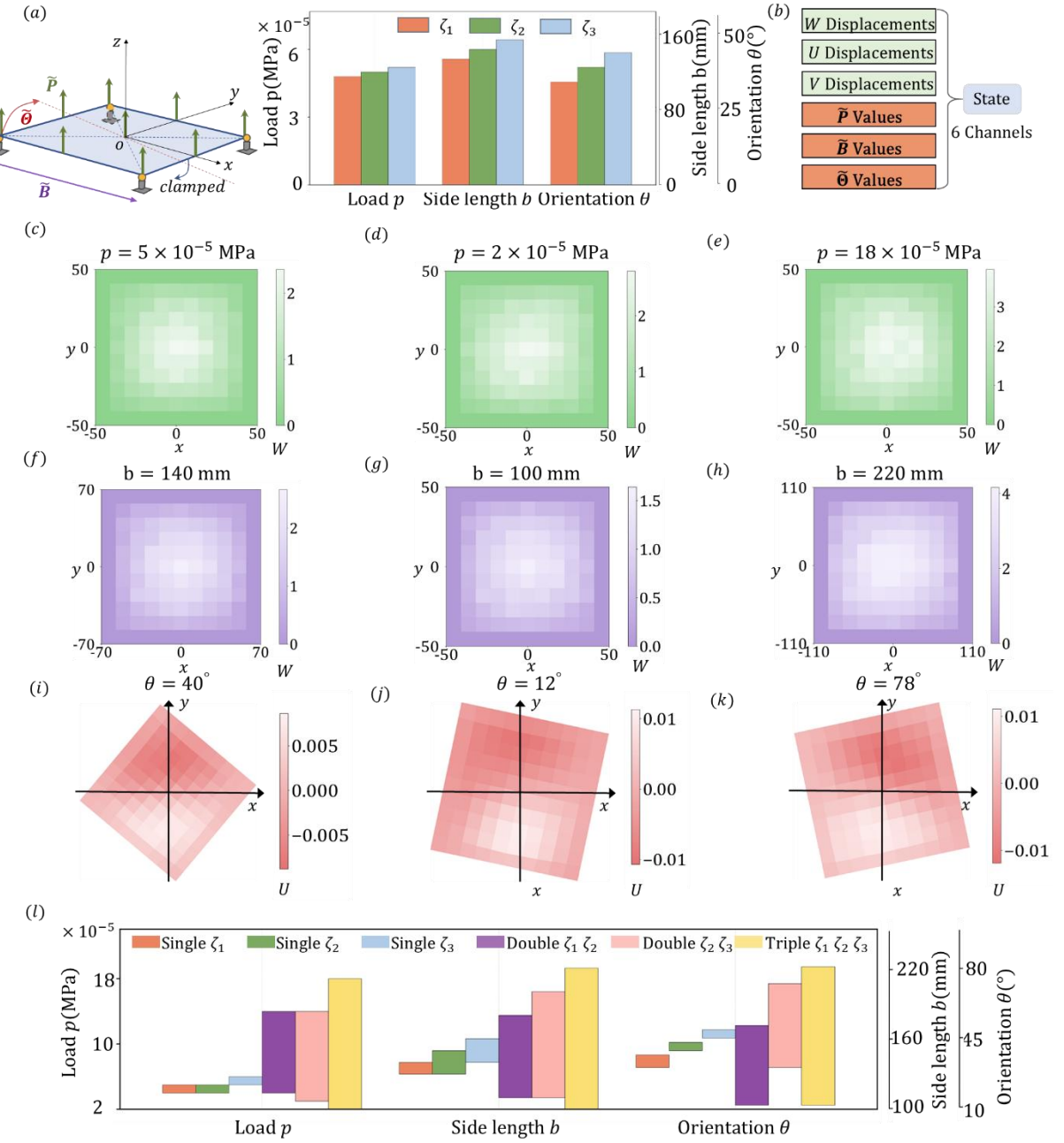


Figure 3. Generalization of episodic observation-switching learning on large-deformation elastic-plate tasks. (a) Left: schematic of the large-deformation elastic plate with clamped edges; right: three closely spaced training observation $\zeta_1, \zeta_2, \zeta_3$ selected for the three tasks, showing only small differences between observations. (b) State representation for the elastic-plate problems, consisting of six channels: out-of-plane displacement W , in-plane displacements U and V , applied load \tilde{P} , plate side length \tilde{B} , and plate orientation $\tilde{\theta}$. (c–e) Task I (varying load): predicted W distributions from a model trained on three nearby \tilde{P} observations, evaluated at the training point ($\tilde{P} = 5 \times 10^{-5}$ MPa) and at two distant test points ($\tilde{P} = 2 \times 10^{-5}$ MPa and 18×10^{-5} MPa), achieving $\bar{R}^2 \approx 0.93$ at the latter. (f–h) Task II (varying plate size): predicted W distributions from the model trained on three similar \tilde{B} observations and evaluated at the training point ($\tilde{B} = 140$ mm) and distant evaluation points ($\tilde{B} = 100$ mm and 200 mm), achieving $\bar{R}^2 \approx 0.93$ at the latter. (i–k) Task III (varying orientation): predicted in-plane displacement U from the model trained on three nearby $\tilde{\theta}$ observations, evaluated at the training point ($\tilde{\theta} = 40^\circ$) and two distant orientations (12° and 78°), with the mean correlation coefficient reaching $\bar{R}^2 \approx 0.92$ at the distant points. (l) Quantitative summary of generalization intervals for all models in all tasks: multi-observation switching training consistently yields substantially enlarged generalization domains relative to single-observation training, indicating an expansion of the generalization domain that exceeds the union of single-observation results.

4. Perspective from Bellman Optimality on Intuitive Learning in DRL

Mechanics intuition, in the context of reinforcement learning, can be formalized as the expectation that the optimal control strategy for a physical system varies smoothly and predictably with changes in continuous physical observation parameters. This implies that small perturbations in a parameter ζ should not lead to abrupt, discontinuous shifts in the optimal value function or policy. We ground this notion in the theoretical framework of Bellman optimality.

4.1. Parameterized Markov Decision Processes

We consider a family of deterministic Markov Decision Processes $M_\zeta = (S_\zeta, A, P, r_\zeta, \gamma)$ parameterized by a physical observation parameter ζ (e.g., load magnitude, geometry). In our design, ζ is explicitly provided as part of the agent's state input. The agent thus learns a parameter-conditioned action-value function $Q_\theta(s, \zeta, a)$ (equivalently $Q_\theta(s(\zeta), a)$).

For each ζ , the Bellman optimality operator B_ζ is defined as

$$(B_\zeta Q)(s, \zeta, a) = \mathbb{E}_{s' \sim P_{\zeta(\cdot|s, a)}} [r(s, \zeta, a) + \gamma \max_{a'} Q(s', \zeta, a')], \quad (1)$$

where P denotes the state transition probability. In our setting, the transition mechanism is not a function of ζ , while the reward r_ζ may depend smoothly on ζ . Under the standard assumptions of bounded rewards and $\gamma \in (0, 1)$, each B_ζ is a contraction mapping in the sup-norm and therefore admits a unique fixed point $Q_\zeta^* = B_\zeta Q_\zeta^*$, which is the optimal value function for the specific physical observation parameter ζ .

4.2. Smoothness of Optimal Solutions Under Parameter Perturbations

A core tenet of our approach is that the mapping $\zeta \mapsto Q_\zeta$ is locally smooth. This can be derived from the perturbation analysis of the Bellman equation. Assuming the reward function r_ζ is Lipschitz continuous in ζ , and noting that the transition dynamics are ζ -independent, a standard contraction mapping argument leads to the bound:

$$\|Q_{\zeta_i}^* - Q_{\zeta_j}^*\|_\infty \leq \frac{C}{1-\gamma} \|\zeta_i - \zeta_j\|. \quad (2)$$

This inequality formalizes the mechanics intuition that nearby physical problems have nearby optimal value functions. Learning a single function Q_θ that accurately approximates Q_ζ^* across a range of ζ is therefore a well-posed problem, provided we can embed this smoothness prior into the learning process.

4.3. Pitfall of Single-Task Training and the Need for Multi-Task Consistency

Training an agent on a single physical observation parameter ζ_k corresponds to minimizing its associated Bellman residual:

$$\mathcal{L}(\theta; \zeta_k) = \mathbb{E}_{(s,a) \sim \mu} \left[\left(Q_\theta(s, \zeta_k, a) - (B_{\zeta_k} Q_\theta)(s, \zeta_k, a) \right)^2 \right]. \quad (3)$$

While this can yield $Q_\theta \approx Q_\zeta^*$ for that specific point, it imposes no constraint on the functions' behavior for $\zeta \neq \zeta_k$. Consequently, the learned Q_θ may overfit, exhibiting arbitrary (non-smooth) variation with ζ , which fails to capture mechanics intuition.

We therefore define the objective of intuitive learning as finding a parameter set θ such that Q_θ simultaneously satisfies (or nearly satisfies) the Bellman optimality conditions for a set of neighboring parameters (e.g., ζ_1, ζ_2, \dots):

$$\sum_k \|Q_\theta(\cdot, \zeta_k, \cdot) - B_{\zeta_k} Q_\theta(\cdot, \zeta_k, \cdot)\|_\infty \approx 0. \quad (4)$$

4.4. Transition to a Unified Geometric View

The preceding analysis establishes that enforcing approximate Bellman consistency across tasks induces local smoothness in the value function. This provides a foundational motivation for our method. To fully explain the emergent generalization capability—why training on merely two or three points yields a disproportionately large region of accuracy—we must examine the underlying structure of the solution space. This leads naturally to a geometric perspective, presented in the next section.

5. Unified Theory of Generalization for Mechanics Intuition via Reinforcement Learning

Building upon the Bellman consistency framework established in Section 4, this section presents a unified theoretical explanation for the strong generalization observed in our experiments. We interpret the continuum of physical tasks as a smooth manifold and show that our training protocol enables the agent to learn a low-dimensional solution submanifold, thereby achieving data-efficient, intuitive generalization.

5.1. The Parameter Manifold and Solution Submanifold

The set of all physical observation parameters ζ defines a smooth parameter manifold \mathcal{M} . Each point $\zeta \in \mathcal{M}$

corresponds to a unique task instance (e.g., a specific brachistochrone endpoint or plate loading condition). Crucially, the family of optimal value functions $\{Q_\zeta^* : \zeta \in \mathcal{M}\}$ does not span the entire high-dimensional function space. Due to the governing physical laws, these solutions lie on or near a low-dimensional submanifold of that space. Learning mechanics intuition is equivalent to approximating this latent solution submanifold.

5.2. Stationarity of the Bellman Residual on Manifold

To formalize the effect of parameter perturbations on the optimal value function, we consider the Bellman optimality equation for the parameterized MDPs. Our framework treats the continuous physical observation parameter ζ (e.g., endpoint coordinates, load magnitude, plate orientation) as a coordinate on a smooth parameter manifold \mathcal{M} , where each point corresponds to a distinct task. The core geometric premise is that the optimal value function $Q^*(s, \zeta, a)$ varies smoothly over \mathcal{M} . To exploit this structure, we restrict training to a small local neighborhood on \mathcal{M} (i.e., $|\zeta_i - \zeta_j|$ is small) and employ episodic observation-switching between neighboring parameters. This protocol implicitly enforces local consistency of the learned $Q_\theta(s, \zeta, a)$ across nearby tasks, effectively biasing the solution toward a smooth submanifold of the function space.

The key theoretical insight is that such smoothness emerges from enforcing stationarity of the Bellman residual with respect to the physical observation parameter $d\delta_{Q_\theta}(\zeta)/d\zeta \approx 0$ where $\delta_{Q_\theta}(\zeta) = Q_\theta - B_\zeta Q_\theta$ is the Bellman residual for parameter ζ . This condition implies that Q_θ varies smoothly with ζ , geometrically confining it to a low-curvature submanifold over \mathcal{M} , and ensuring that the learned policy generalizes coherently across tasks rather than memorizing isolated solutions.

The empirical evidence is consistent with this view: on both the brachistochrone and the elastic-plate problems, episodic switching across a few neighboring observations yields a generalization region that substantially exceeds the union of single-task training intervals. To formalize this phenomenon, we now analyze how a small perturbation of ζ propagates through the Bellman optimality equation, thereby deriving the stationarity condition and establishing a theoretical foundation for the data-efficient, intuition-like generalization observed in our experiments.

We still consider a family of parameterized MDP indexed by a continuous physical observation parameter ζ .

Denote by $P_\zeta(\cdot | s, a)$ the transition kernel (which reduces to a deterministic mapping in physics-based environments) and by $r(s(\zeta), a, s'(\zeta))$ the immediate reward under parameter ζ . The optimal action-value function $Q^*(s(\zeta), a)$ satisfies the Bellman optimality equation in expectation form

$$Q^*(s(\zeta), a) = \mathbb{E}_{s' \sim P_{\zeta(\cdot | s, a)}} [r(s(\zeta), a, s'(\zeta)) + \gamma \max_{a'} Q^*(s'(\zeta), a'(\zeta))], \quad (5)$$

with the discount factor $\gamma \in (0, 1)$. We assume that $Q^*(s(\zeta), a)$ and $r(s(\zeta), a, s'(\zeta))$ are locally differentiable with respect to ζ and that the maximizing action remains unchanged under sufficiently small perturbations of ζ (so that the $\max_{a'} Q^*(s'(\zeta), a'(\zeta))$ can be treated by same-action differentiation). This assumption is reasonable for continuous physical systems where the underlying optimal policy varies smoothly with ζ over local neighborhoods of \mathcal{M} . For a nearby environment parameter $\zeta + \Delta\zeta$, the corresponding Bellman equation reads

$$Q^*(s(\zeta + \Delta\zeta), a) = \mathbb{E}_{s' \sim P_{\zeta + \Delta\zeta(\cdot | s, a)}} [r(s(\zeta + \Delta\zeta), a, s'(\zeta + \Delta\zeta)) + \gamma \max_{a'} Q^*(s'(\zeta + \Delta\zeta), a'(\zeta + \Delta\zeta))]. \quad (6)$$

Applying a first-order Taylor expansion with respect to ζ yields

$$Q^*(s(\zeta), a) + \frac{dQ^*(s(\zeta), a)}{d\zeta} \cdot \Delta\zeta = \mathbb{E}_{s' \sim P_{\zeta + \Delta\zeta(\cdot | s, a)}} \left[r(s(\zeta), a, s'(\zeta)) + \frac{dr(s(\zeta), a, s'(\zeta))}{d\zeta} \cdot \Delta\zeta + \gamma \left(\max_{a'} Q^*(s'(\zeta), a') + \frac{d\max_{a'} Q^*(s'(\zeta), a')}{d\zeta} \cdot \Delta\zeta \right) \right]. \quad (7)$$

Subtracting Eq. (5) from Eq. (7) and dividing both sides by $\Delta\zeta$, we obtain

$$\begin{aligned} & \frac{dQ^*(s(\zeta), a)}{d\zeta} \cdot \Delta\zeta \\ &= \mathbb{E}_{s' \sim P_{\zeta(\cdot | s, a)}} \left[\frac{dr(s(\zeta), a, s'(\zeta))}{d\zeta} \cdot \Delta\zeta + \gamma \frac{d\max_{a'} Q^*(s'(\zeta), a')}{d\zeta} \cdot \Delta\zeta \right] \\ &+ \mathbb{E}_{s' \sim P_{\zeta + \Delta\zeta(\cdot | s, a)} - P_{\zeta(\cdot | s, a)}} \left[r(s(\zeta), a, s'(\zeta)) + \frac{dr(s(\zeta), a, s'(\zeta))}{d\zeta} \cdot \Delta\zeta \right. \\ & \quad \left. + \gamma \left(\max_{a'} Q^*(s'(\zeta), a') + \frac{d\max_{a'} Q^*(s'(\zeta), a')}{d\zeta} \cdot \Delta\zeta \right) \right], \end{aligned} \quad (8)$$

where the last term collects the effect of the change in the transition law $\Delta P := P_{\zeta + \Delta\zeta} - P_\zeta$.

This condition is exactly satisfied in our formulation: since the physical observation parameter ζ is explicitly encoded as part of the input state $s(\zeta)$, the transition dynamics become independent of ζ (i.e., $P_{\zeta + \Delta\zeta}(\cdot | s, a) = P_\zeta(\cdot | s, a)$). Consequently, the distributional term vanishes ($\Delta P \equiv 0$). Under this mild and verifiable modeling choice the decomposition (8) simplifies to

$$\frac{dQ^*(s(\zeta), a)}{d\zeta} = \mathbb{E}_{s' \sim P_{\zeta(\cdot|s, a)}} \left[\frac{dr(s(\zeta), a, s'(\zeta))}{d\zeta} + \gamma \frac{d\max_{a'} Q^*(s'(\zeta), a')}{d\zeta} \right]. \quad (9)$$

Rearranging gives the derivative-form stationarity of the Bellman residual

$$\frac{d\delta_Q(\zeta)}{d\zeta} = 0, \quad (10)$$

where the Bellman residual $\delta_Q(\zeta) = Q^*(s(\zeta), a) - \mathbb{E}_{s' \sim P_{\zeta(\cdot|s, a)}} [r(s(\zeta), a, s'(\zeta)) + \gamma \max_{a'} Q^*(s'(\zeta), a')]$.

For the optimal solution Q^* , the Bellman residual vanishes identically for all ζ , and Eq. (10) holds trivially. However, during learning we instead optimize a parameterized approximation Q_θ , where θ denotes the network parameters. In this case, Eq. (10) implies that a necessary condition for accurately approximating the optimal solution over a neighborhood of ζ is that the Bellman residual varies smoothly with respect to the physical observation parameter:

$$\frac{d\delta_{Q_\theta}(\zeta)}{d\zeta} \approx 0. \quad (11)$$

Eq. (11) shows that the Bellman residual of the optimal solution is stationary with respect to the physical observation parameter ζ . This stationarity condition is a necessary (though not sufficient) requirement for learning a smooth value function approximation over ζ . Under the local smooth manifold assumption, however, it suffices to guide the network to capture the local geometry of the solution submanifold. While this condition holds identically for the true optimal function Q^* , it becomes nontrivial when considering a learned approximation Q_θ . In practice, the model is trained by alternately minimizing Bellman residuals at a finite set of nearby parameters ζ_i . For two similar parameters ζ_i and ζ_j , this procedure implicitly enforces the finite-difference constraint

$$\frac{\delta_{Q_\theta}(\zeta_i) - \delta_{Q_\theta}(\zeta_j)}{\zeta_i - \zeta_j} \approx 0, \quad (12)$$

which serves as a discrete approximation to the derivative condition in Eq. (11). Consequently, in episodic observation-switching training, the network parameters θ are alternately optimized to minimize the Bellman residual at multiple nearby environments ζ_i . This procedure not only enforces δQ_θ at each sampled environment, but also implicitly minimizes the finite-difference approximation of the residual derivative in Eq. (12).

As a result, the learned action–value function is constrained to lie on a low-curvature manifold with respect to ζ ,

capturing the local structure of the entire solution family rather than memorizing isolated solutions. This explains why episodic observation-switching training on multiple highly similar observations yields a generalization interval that is substantially larger than the union of the generalization regions obtained from single-observation training. In particular, ensuring the continuity of the Bellman residual across neighboring parameters provides a theoretical explanation for the stable and robust mechanics intuition exhibited by the agent during episodic observation-switching training.

5.3. Algorithmic Mechanism: Experience Mixing as Implicit Regularization

The episodic switching protocol has a critical implementation-level consequence: the shared experience replay buffer \mathcal{D} is populated with transition tuples (s, a, r, s') collected under different physical observation parameters ζ_i and ζ_j . Consequently, when a minibatch is sampled from \mathcal{D} for Q-network optimization, it naturally constitutes a mixture of experiences from neighboring tasks. This forces each gradient update to simultaneously reduce the Bellman residual across multiple ζ values. The optimization is thereby biased against solutions that are optimal for a single ζ but highly inconsistent for a nearby ζ ; instead, it steers the network parameters θ toward a unified solution that approximately satisfies the Bellman optimality conditions for the entire local cluster. This implicit multi-task learning through experience mixing is the algorithmic mechanism that materializes the mathematical smoothness constraint (Eq. (12)) and underpins the geometric intuition of learning a coherent function on the parameter manifold.

5.4. Explaining the Generalization Gain

This unified theory directly explains the key computational findings. Single-observation training generalizes poorly because it minimizes δ_{Q_θ} only at an isolated point on \mathcal{M} , with no constraint on the function's behavior elsewhere. The learned Q_θ is not anchored to the solution submanifold, leading to rapid degradation away from the training point.

Switching between few similar observations generalizes widely because training on a local cluster $\zeta_1, \zeta_2, \zeta_3$ enforces residual stationarity (via Eq. (12)) within that neighborhood. These forces Q_θ to approximate the local tangent structure of the solution submanifold. Once the local geometry is captured, the function can extrapolate reliably along the manifold, generating accurate predictions for distant ζ_{test} that share the same underlying physical structure. The generalization region thus expands non-additively, covering a continuous portion of \mathcal{M} rather than just the union of

isolated point neighborhoods. This theoretical mechanism directly explains the nonlinear expansion of the high-accuracy region observed in Fig. 2(c–e) and Fig. 3(l), where training on a local cluster of tasks yields generalization far beyond the union of single-task training intervals.

5.5. Connection to Broader Themes

This framework bridges our method with concepts in geometric deep learning and few-shot learning. The parameter manifold \mathcal{M} acts as a physics-informed prior, and episodic switching is a curriculum that induces a data-driven coordinate chart for the solution submanifold. This perspective suggests future pathways, such as incorporating explicit manifold-regularization terms or meta-learning the manifold structure, to further enhance generalization in high-dimensional parameter spaces.

Notably, the generality of our framework extends well beyond classical mechanics. The core methodology—encoding continuous physical parameters into the state and using the physical functional as the reward signal—is domain-agnostic. It can be directly applied to any optimization problem governed by a known scalar functional. This includes diverse fields such as electromagnetics (e.g., field-shaping for minimal radiation loss), thermodynamics (e.g., heat conduction path optimization), and fluid dynamics (e.g., drag minimization in shape design).

Remarkably, it also extends to quantum-mechanical problems, where the functional is often an expectation value of a Hamiltonian. For instance, finding ground-state wavefunctions or optimizing quantum control pulses can be formulated as RL tasks where the agent iteratively adjusts parameters (e.g., variational ansatz coefficients or pulse shapes) to minimize energy or maximize fidelity. The episodic switching protocol could then help the agent generalize across a family of related Hamiltonians or target states. This potential connection underscores that our framework is not merely a tool for classical mechanics, but a unified approach for building parameter-conditioned intuition across the physical sciences, wherever a well-defined objective functional exists.

6. Conclusions

By encoding physical parameters into the state and switching between related tasks during training, our method enables the agent to extract and reuse shared structures, thus acquiring broad mechanics intuition from few examples.

Theoretically, this is achieved by enforcing stationarity of the Bellman residual across parameters, which biases the learner towards a consistent value function over the task family.

Geometrically, our method learns a smooth function over the task parameter manifold, ensuring generalization. This success stems from two synergistic components: a physics-informed smoothness prior, instantiated by sampling closely related tasks, and the episodic switching protocol, which mixes experiences across tasks and acts as an implicit regularizer. The prior defines the low-dimensional solution structure to be learned; the switching protocol enables its acquisition from scarce data. Ultimately, the learning process is constrained such that small task variations preserve Bellman consistency, naturally promoting generalization.

These findings offer a computational perspective on how data-efficient mechanics intuition might emerge in both artificial and biological systems, through continual interaction with environment. In cognitive science, human generalization is often described as the abstraction of conceptual models from sparse examples [5]. While the underlying mechanisms are undoubtedly different, our RL agent exhibits a functionally similar capability: by encoding parameters and enforcing Bellman consistency, it develops a policy that generalizes across a continuous task family, as if it had formed an abstract, parameterized model of the underlying physics. This suggests that enforcing consistency across related experiences—whether through cognitive abstraction or through algorithmic constraints like stationary Bellman residuals—may be a general principle for efficient learning.

Thus, our work not only demonstrates strong generalization in physical task families but also provides a unifying computational principle: maintaining coherence across related tasks is key to extracting broad insights from limited data. This principle aligns with insights from neuroscience-inspired AI, where structural biases (e.g., recurrent circuits [24]) can also promote generalization. Future research could explore whether such algorithmic principles can inform our understanding of biological learning, or conversely, how biological insights might further refine data-efficient RL.

While our approach requires a known physical functional, its integration with data-driven physics discovery [25,26] (e.g., PINNs [27–31], symbolic regression [32,33]) can directly address scenarios with unknown laws. A synergistic pathway emerges: first discover the governing functional from data [34,35], then apply our RL framework to optimize

within the learned model. This hybrid paradigm extends our method to problems lacking analytic first principles, effectively bridging data-driven discovery and model-based RL control.

Reference

- [1] M. K. Eckstein, L. Wilbrecht, and A. G. Collins, What do reinforcement learning models measure? Interpreting model parameters in cognition and neuroscience, *Value Based Decis.-Mak.* **41**, 128 (2021).
- [2] T. H. Muller, J. L. Butler, S. Veselic, B. Miranda, J. D. Wallis, P. Dayan, T. E. J. Behrens, Z. Kurth-Nelson, and S. W. Kennerley, Distributional reinforcement learning in prefrontal cortex, *Nat. Neurosci.* **27**, 403 (2024).
- [3] R. Hattori, N. G. Hedrick, A. Jain, S. Chen, H. You, M. Hattori, J.-H. Choi, B. K. Lim, R. Yasuda, and T. Komiyama, Meta-reinforcement learning via orbitofrontal cortex, *Nat. Neurosci.* **26**, 2182 (2023).
- [4] L. S. Piloto, A. Weinstein, P. Battaglia, and M. Botvinick, Intuitive physics learning in a deep-learning model inspired by developmental psychology, *Nat. Hum. Behav.* **6**, 1257 (2022).
- [5] H. Tiedemann, Y. Morgenstern, F. Schmidt, and R. W. Fleming, One-shot generalization in humans revealed through a drawing task, *eLife* **11**, e75485 (2022).
- [6] K. M. Collins et al., Building machines that learn and think with people, *Nat. Hum. Behav.* **8**, 1851 (2024).
- [7] J. B. Tenenbaum, C. Kemp, T. L. Griffiths, and N. D. Goodman, How to Grow a Mind: Statistics, Structure, and Abstraction, *Science* **331**, 1279 (2011).
- [8] M. Malaviya, I. Sucholutsky, K. Oktar, and T. L. Griffiths, *Can Humans Do Less-Than-One-Shot Learning?*, in (2022).
- [9] A. Bhoopchand et al., Learning few-shot imitation as cultural transmission, *Nat. Commun.* **14**, 7536 (2023).
- [10] B. M. Lake and M. Baroni, Human-like systematic generalization through a meta-learning neural network, *Nature* **623**, 115 (2023).
- [11] J. Peng and S. Zhu, Developing artificial mechanics intuitions from extremely small data, *Extreme Mech. Lett.* **78**, (2025).
- [12] R. Zhao et al., A framework for the general design and computation of hybrid neural networks, *Nat. Commun.* **13**, 3427 (2022).
- [13] S. Casper et al., *Open Problems and Fundamental Limitations of Reinforcement Learning from Human Feedback*, arXiv:2307.15217.
- [14] Y. Meng, Z. Bing, X. Yao, K. Chen, K. Huang, Y. Gao, F. Sun, and A. Knoll, Preserving and combining knowledge in robotic lifelong reinforcement learning, *Nat. Mach. Intell.* **7**, 256 (2025).
- [15] T. Wise, K. Emery, and A. Radulescu, Naturalistic reinforcement learning, *Trends Cogn. Sci.* **28**, 144 (2024).
- [16] A. Gupta, S. Savarese, S. Ganguli, and L. Fei-Fei, Embodied intelligence via learning and evolution, *Nat. Commun.* **12**, 5721 (2021).
- [17] Y. Meng, Z. Bing, X. Yao, K. Chen, K. Huang, Y. Gao, F. Sun, and A. Knoll, Preserving and combining knowledge in robotic lifelong reinforcement learning, *Nat. Mach. Intell.* **7**, 256 (2025).
- [18] L. Ouyang et al., *Training Language Models to Follow Instructions with Human Feedback*, in *Advances in Neural Information Processing Systems*, edited by S. Koyejo, S. Mohamed, A. Agarwal, D. Belgrave, K. Cho, and A. Oh, Vol. 35 (Curran Associates, Inc., 2022), pp. 27730–27744.
- [19] J. Oh, G. Farquhar, I. Kemaev, D. A. Calian, M. Hessel, L. Zintgraf, S. Singh, H. van Hasselt, and D. Silver, Discovering state-of-the-art reinforcement learning algorithms, *Nature* **648**, 312 (2025).
- [20] D. Guo et al., DeepSeek-R1 incentivizes reasoning in LLMs through reinforcement learning, *Nature* **645**, 633

(2025).

- [21] H. Yu, I. Mineyev, L. R. Varshney, and J. A. Evans, Learning from one and only one shot, *Npj Artif. Intell.* **1**, 13 (2025).
- [22] M. Steyvers, H. Tejeda, A. Kumar, C. Belem, S. Karny, X. Hu, L. W. Mayer, and P. Smyth, What large language models know and what people think they know, *Nat. Mach. Intell.* **7**, 221 (2025).
- [23] R. Hattori, N. G. Hedrick, A. Jain, S. Chen, H. You, M. Hattori, J.-H. Choi, B. K. Lim, R. Yasuda, and T. Komiyama, Meta-reinforcement learning via orbitofrontal cortex, *Nat. Neurosci.* **26**, 2182 (2023).
- [24] D. Pedamonti, S. Mohinta, M. V. Dimitrov, H. Malagon-Vina, S. Ciocchi, and R. P. Costa, Hippocampus supports multi-task reinforcement learning under partial observability, *Nat. Commun.* **16**, 9619 (2025).
- [25] W. Song, S. Jiang, G. Camps-Valls, M. Williams, L. Zhang, M. Reichstein, H. Vereecken, L. He, X. Hu, and L. Shi, Towards data-driven discovery of governing equations in geosciences, *Commun. Earth Environ.* **5**, 589 (2024).
- [26] H. Xu, Y. Chen, R. Cao, T. Tang, M. Du, J. Li, A. H. Callaghan, and D. Zhang, Generative discovery of partial differential equations by learning from math handbooks, *Nat. Commun.* **16**, 10255 (2025).
- [27] Z. Chen, Y. Liu, and H. Sun, Physics-informed learning of governing equations from scarce data, *Nat. Commun.* **12**, 6136 (2021).
- [28] F. Wang, Z. Zhai, Z. Zhao, Y. Di, and X. Chen, Physics-informed neural network for lithium-ion battery degradation stable modeling and prognosis, *Nat. Commun.* **15**, 4332 (2024).
- [29] Z. Liu, Y. Liu, X. Yan, W. Liu, H. Nie, S. Guo, and C. Zhang, Automatic network structure discovery of physics informed neural networks via knowledge distillation, *Nat. Commun.* **16**, 9558 (2025).
- [30] K. Luo, J. Zhao, Y. Wang, J. Li, J. Wen, J. Liang, H. Soekmadji, and S. Liao, Physics-informed neural networks for PDE problems: a comprehensive review, *Artif. Intell. Rev.* **58**, 323 (2025).
- [31] G. E. Karniadakis, I. G. Kevrekidis, L. Lu, P. Perdikaris, S. Wang, and L. Yang, Physics-informed machine learning, *Nat. Rev. Phys.* **3**, 422 (2021).
- [32] C. Cornelio, S. Dash, V. Austel, T. R. Josephson, J. Goncalves, K. L. Clarkson, N. Megiddo, B. El Khadir, and L. Horesh, Combining data and theory for derivable scientific discovery with AI-Descartes, *Nat. Commun.* **14**, 1777 (2023).
- [33] J. Hu, J. Cui, and B. Yang, Learning interpretable network dynamics via universal neural symbolic regression, *Nat. Commun.* **16**, 6226 (2025).
- [34] Z. Liu and M. Tegmark, Machine Learning Conservation Laws from Trajectories, *Phys. Rev. Lett.* **126**, 180604 (2021).
- [35] X. Fu, Z. Liu, and M. Tegmark, *Do Two AI Scientists Agree?*, arXiv:2504.02822.